Topics in Catalysis (2018) 61:1537–1544
https://doi.org/10.1007/s11244-018-0965-7

ORIGINAL PAPER

CO and CO_2 Methanation Over Ni/SiC and Ni/SiO_2 Catalysts

Thien An Le[1] · Jong Kyu Kang[1] · Eun Duck Park[1]

Published online: 20 April 2018

Abstract
Ni/SiC and Ni/SiO_2 catalysts prepared by both wet impregnation (WI) and deposition–precipitation (DP) methods were compared for CO and CO_2 methanation. The prepared catalysts were characterized using N_2 physisorption, temperature-programmed reduction with H_2 (H_2-TPR), H_2 chemisorption, pulsed CO_2 chemisorption, temperature-programmed desorption of CO_2 (CO_2-TPD), transmission electron microscopy, and X-ray diffraction. H_2-TPR analysis revealed that the catalysts prepared by DP exhibit stronger interaction between the nickel oxides and support than those prepared by WI. The former catalysts exhibit higher Ni dispersions than the latter. The catalytic activities for both reactions over Ni/SiC and Ni/SiO_2 catalysts prepared by WI increase on increasing the Ni content from 10 to 20 wt%. The Ni/SiC catalyst prepared by DP shows higher catalytic activity for CO and CO_2 methanation than that of the Ni/SiC catalyst prepared by WI. Furthermore, it exhibits the highest catalytic activity for CO methanation among the tested catalysts. The high Ni dispersion achieved by the DP method and the high thermal conductivity enabled by SiC are beneficial for both CO and CO_2 methanation.

Keywords CO methanation · CO_2 methanation · Ni/SiC · Ni/SiO_2 · Deposition–precipitation method

1 Introduction

CO methanation is an important chemical reaction for transforming synthesis gas, a mixture of CO and hydrogen, into synthetic natural gas:

$$CO(g) + 3H_2(g) \leftrightarrow CH_4(g) + H_2O(g) \Delta H^{o}_{(298K)} = -206 \text{ kJ/mol} \quad (1)$$

This reaction can be used to increase the value of biomass, coal, and organic waste by gasification or to utilize the gas byproducts from the steel industry [1, 2].

CO_2 methanation is considered to be a promising reaction for utilizing CO_2 and reducing global warming due to anthropogenic CO_2 emissions:

$$CO_2(g) + 4H_2(g) \leftrightarrow CH_4(g) + 2H_2O(g) \Delta H^{o}_{(298K)} = -165 \text{ kJ/mol} \quad (2)$$

This reaction exemplifies the power-to-gas concept, in which CO_2 separated from the atmosphere and hydrogen generated from water using renewable energy are converted into methane that can be transported and distributed through the gas grid [3].

Since these reactions are highly exothermic and thermodynamically limited at high temperatures, catalysts that exhibit high activity at low temperatures and catalyst beds with efficient heat transfer are required for designing compact reactors capable of high single-pass conversion. High catalytic activity and effective heat transfer are closely related to the active metal and support material in a catalyst, respectively. Ni is commonly used as the active metal in commercial catalysts because of its comparatively low price and high intrinsic catalytic activity [4–10].

The support material is the most important component in a catalyst besides the active component and promoter. Its major role is to disperse the active component, which can be, for instance, a metal, metal oxide, metal sulfide, or metal nitride. For practical applications, other important factors such as mechanical and thermal properties should be considered when selecting a support material that is appropriate for the active component and target reaction. A support material with high thermal conductivity is critical for highly exothermic or endothermic reactions in order to avoid hot spots in

Electronic supplementary material The online version of this article (https://doi.org/10.1007/s11244-018-0965-7) contains supplementary material, which is available to authorized users.

✉ Eun Duck Park
edpark@ajou.ac.kr

[1] Department of Chemical Engineering and Department of Energy Systems Research, Ajou University, 206, World cup-ro, Yeongtong-Gu, Suwon 16499, Republic of Korea

the catalyst bed or a significant radial temperature gradient in the reactor. In this respect, conventional ceramic supports such as alumina, silica, and zeolites are less favorable for these reactions than high-thermal-conductivity materials such as carbon, metal monoliths, and silicon carbide (SiC).

SiC exhibits high thermal conductivity, high resistance to oxidizing conditions, a relatively high surface area without micropores, and chemical inertness [11–14]. Consequently, SiC has been applied as a catalyst support in a variety of highly exothermic and endothermic reactions, such as partial oxidation [12], the Fischer–Tropsch synthesis [15], oxidative coupling of methane [16], and methane reforming [17, 18]. A variety of supports with large surface areas and high thermal stabilities have been applied to CO and CO_2 methanation, including CeO_2, ZrO_2, γ-Al_2O_3, SiO_2, and TiO_2 [19–24]. For example, Zhang et al. [25] prepared Ni/SiC and Ni/Al_2O_3 catalysts by the impregnation method and compared their catalytic activities for CO methanation. They found that the Ni/SiC catalyst exhibited more stable catalytic activity than the Ni/Al_2O_3 catalyst, even though the former contained larger Ni particles than the latter. Furthermore, Jin et al. [26] prepared various Ni/Al_2O_3/SiC catalysts with different Al contents by the co-deposition-precipitation method and applied them to CO methanation. They concluded that the addition of Al_2O_3 is beneficial to catalytic activity and stability. However, to the best of our knowledge, no studies comparing Ni/SiC and Ni/SiO_2 catalysts for CO and CO_2 methanation have been reported.

In this study, we have found that, along with the choice of support materials, the catalyst preparation method also exerts an important effect on catalytic activity. The Ni/SiC catalyst prepared by the deposition–precipitation (DP) method shows a higher catalytic activity for CO methanation than that of the Ni/SiO_2 catalyst, which has a much higher surface area. The former catalyst also exhibits comparable catalytic activity with that of the latter for CO_2 methanation. The effect of the support material on CO and CO_2 methanation activity in the presence of a promoter was also investigated. To that end, manganese was chosen as an effective promoter, allowing a direct comparison of the catalytic activities of Mn–Ni/SiC and Mn–Ni/SiO_2 catalysts, because the addition of Mn to Ni catalysts has been reported to increase Ni dispersion [27] and provide a higher oxygen vacancy concentration [28], resulting in outstanding catalytic performance for CO methanation.

2 Experimental

2.1 Preparation of Catalysts

Two different supports, SiO_2 (Zeochem, ZEOprep 60) and SiC (US Nano), were purchased and used as received. The supported Ni catalysts were prepared with the wet impregnation (WI) method or deposition–precipitation (DP) method. In the case of WI, a specific amount of $Ni(NO_3)_2{\cdot}6H_2O$ (Junsei Chemical Co., Ltd.) was dissolved in 50 mL deionized water and mixed with 5 g support. The excess water was slowly removed using a rotary evaporator (BUCHI, Switzerland). The recovered powder was dried in an oven at 120 °C for 12 h and then calcined in an air stream at 500 °C for 3 h. For the DP method, the specific amount of $Ni(NO_3)_2{\bullet}6H_2O$ (Junsei Chemical Co., Ltd.) was dissolved in 50 mL deionized water. This solution was brought into contact with the support and mixed with a urea solution, in which the molar ratio of nickel:urea was fixed at 1:2, for 16 h by stirring at 90 °C to allow urea decomposition. The entire precipitation process was performed in a closed vessel. The powder recovered after filtering was dried in an oven at 110 °C for 12 h and calcined in an air stream at 500 °C for 3 h. The same procedure was adopted to prepare the Mn-promoted supported Ni catalysts except that the molar ratio of Mn:Ni was fixed at 1:10. $Mn(NO_3)_2{\cdot}4H_2O$ (Sigma–Aldrich) was used as the Mn precursor. All the calcined samples were reduced in a H_2 stream at 500 or 600 °C for 1 h before reaction. In order to distinguish each catalyst, the Ni content and preparation method are indicated by the name of the catalyst, for example, 10Ni/SiC-WI indicates a Ni catalyst supported on SiC prepared by the WI method containing 10 wt% Ni. For the catalyst reduced at 600 °C, the reduction temperature is also given. For example, 20Ni/SiO_2-DP (600) denotes a 20 wt% Ni catalyst supported on SiO_2 prepared by DP and reduced at 600 °C.

2.2 Characterization of Catalysts

N_2 physisorption, temperature-programmed reduction with H_2 (H_2-TPR), H_2 chemisorption, pulsed CO_2 chemisorption, temperature-programmed desorption of CO_2 (CO_2-TPD), transmission electron microscopy (TEM), and X-ray diffraction (XRD) were used to characterize the prepared catalysts. All the procedures are described in detail in the Supporting Information.

2.3 Catalytic Activity Tests

The catalytic activity tests were performed at atmospheric pressure using a continuous fixed-bed reactor system as described in the Supporting Information. Briefly, 0.10 g of the catalyst was loaded into the quartz reactor and brought into contact with a feed composed of 1 mol% CO or CO_2, 50 mol% H_2, and 49 mol% He at a flow rate of 100 mL/min.

3 Results and Discussion

3.1 Characterization of the Catalysts

The physicochemical properties of the Ni catalysts supported on SiO_2 and SiC are presented in Table 1. The BET surface area of SiC is approximately one-tenth that of SiO_2. Neither support has micropores. The average pore diameters of SiC and SiO_2 were determined to be 9 and 6 nm, respectively. In the case of the SiO_2-supported Ni catalysts, their surface areas decrease with the incorporation of Ni onto the support while maintaining their average pore diameters. This implies that the loaded Ni species are well dispersed throughout the support without pore plugging. Conversely, there is no noticeable decrease in the surface area of the Ni/SiC-WI catalysts, irrespective of Ni content. Note that the surface area of Ni/SiC-DP increases to approximately four-times that of SiC. This indicates that the deposited Ni species contribute to an increase in the surface area of the catalyst.

The nitrogen adsorption and desorption data in Fig. S1 show that the Ni/SiC and Ni/SiO_2 catalysts have type III and type IV isotherms, respectively [30]. This implies that the interaction between nitrogen and SiC is relatively weak and that the adsorbed nitrogen molecules are clustered around the most favorable sites on the surface of the nonporous or macroporous SiC [30]. For the Ni/SiC-DP catalyst, a type H3 loop is observed, which originates from a pore network consisting of macropores that are not completely filled with pore condensate [30]. Conversely, all Ni/SiO_2 catalysts exhibit type H2(b) loops, which are frequently observed for mesoporous silica [30]. The pore size distribution of each catalyst is also given in Fig. S2. A broad pore size distribution ranging from 3 to 10 nm is observed for the Ni/SiO_2-WI catalysts. The Ni/SiC-WI catalysts have a bimodal pore size distribution in which a sharp peak at 4 nm and a broad peak from 6 to 120 nm with a maximum at 40 nm are observed. However, all the supported Ni catalysts prepared by DP present the sharp peak at ~ 4 nm in the pore size distribution. This indicates that these pores develop, while other pores are blocked during the DP process.

In order to investigate the bulk crystalline structures of the catalysts, XRD patterns were obtained for all the calcined and reduced catalysts. For all supported Ni catalysts prepared by WI and calcined at 500 °C, strong XRD peaks corresponding to NiO were observed and these peak intensities were strengthened with increasing Ni content from 10 to 20 wt% (Fig. S3). On the other hand, no XRD peak due to NiO can be observed for all supported Ni catalysts prepared by DP and calcined at 500 °C. This indicates that Ni oxides are highly dispersed on the support for calcined Ni/SiC-DP and Ni/SiO_2-DP samples. In the case of Ni/SiO_2-DP calcined at 500 °C, very weak XRD peaks corresponding to nickel antigorite ($Ni_3Si_2O_5(OH)_4$) were detected (Fig. S3). As shown in Fig. 1, strong XRD peaks corresponding to metallic Ni are observed only for the supported Ni catalysts prepared by WI and reduced at 500 °C. The crystallite size of Ni in Ni/SiC-WI was calculated to be much larger than that in Ni/SiO_2-WI (Table 1). There is no significant change in the crystallite size of Ni in the Ni catalysts supported on the same support upon increasing the Ni content from 10 to 20 wt%. This is consistent with the Ni dispersion determined by H_2 chemisorption (Table 1). No XRD peaks attributed to metallic Ni are observed for Ni/SiC-DP or Ni/SiO_2-DP both reduced at 500 °C (Fig. 1b), indicating that the Ni species are well dispersed over the supports in these catalysts.

Table 1 Physicochemical properties of support materials and supported Ni catalysts

Catalyst	Specific surface area (m^2/g)[a]	Pore volume (cm^3/g)[a]	Average pore diameter (nm)[a]	Ni dispersion (%)[b]	CASA ($m^2/g_{cat.}$)[b]	Crystallite size of Ni (nm)[c]
SiO_2	477	0.73	6	–	–	–
SiC	43	0.09	9	–	–	–
10Ni/SiO_2-WI	380	0.58	5	1.9	1.3	11
20Ni/SiO_2-WI	322	0.45	6	1.9	2.5	12
10Ni/SiC-WI	59	0.22	15	1.1	0.7	22
20Ni/SiC-WI	48	0.23	20	1.5	2.0	22
20Ni/SiO_2-DP	358	0.48	5	7.1	9.4	n.d
20Ni/SiC-DP	164	0.60	15	8.1	10.8	n.d

All catalysts were calcined in air and reduced in hydrogen at 500 °C

n.d. not detected

[a]Specific surface area, pore volume, and average pore diameter were determined by N_2 physisorption

[b]Ni dispersion and CASA were determined based on H_2 chemisorption data

[c]Crystallite size of Ni was calculated based on XRD data using the Scherrer formula [29]

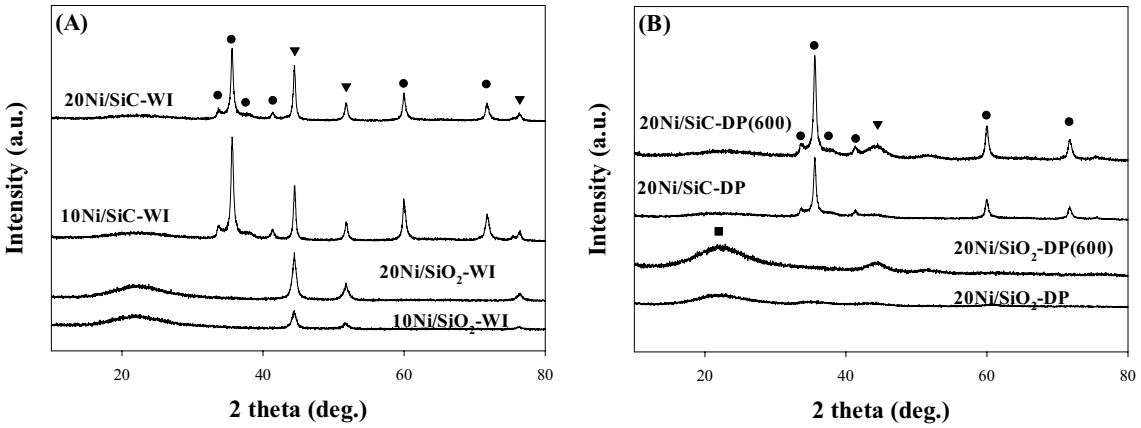

Fig. 1 XRD patterns of supported Ni catalysts **a** prepared by WI then reduced at 500 °C, and **b** prepared by DP then reduced at 500 or 600 °C. (filled circle) SiC (JCPDS 29-1129), (filled inverted triangle) Ni (JCPDS 04-0850), and (filled square) SiO_2 (JCPDS 71-0785)

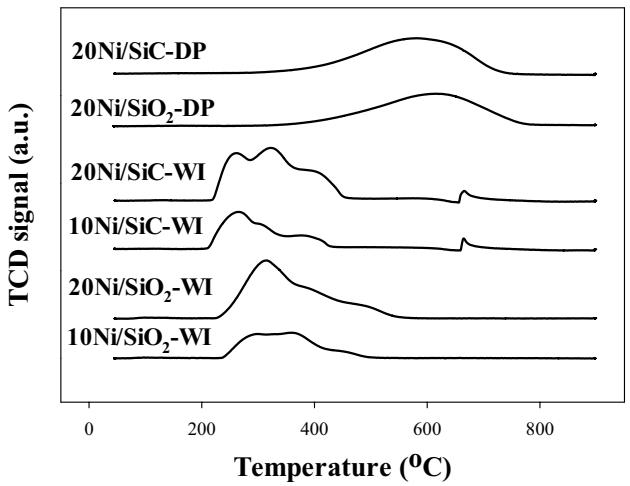

Fig. 2 H_2-TPR profiles of supported Ni catalysts calcined at 500 °C

Higher Ni dispersions were measured for the catalysts prepared by DP than for those prepared by WI (Table 1). Weak XRD peaks corresponding to metallic Ni are observed for the supported Ni catalysts prepared by DP and reduced at 600 °C (Fig. 1b). However, the crystallite size of the Ni could not be determined because of the low peak intensity, indicating that the metallic Ni particles are highly dispersed on the support, even after reduction at 600 °C.

To assess the reducibility of nickel oxides on different supports, H_2-TPR patterns were obtained for supported Ni catalysts calcined in air at 500 °C, as shown in Fig. 2. In the case of the catalysts prepared by WI, the onset of the TPR peak is observed at a lower temperature for the SiC-supported Ni catalysts than that for the SiO_2-supported Ni catalysts. This implies that the interaction between the Ni oxides and the support is weaker for SiC than that for SiO_2. Generally, the weaker interaction between metal oxides and the support results in the formation of large metal particles after reduction. As shown in Table 1, the larger crystallite size of Ni was obtained for the SiC-supported Ni catalysts than that for the SiO_2-supported Ni catalysts prepared by WI. This is consistent with the TPR data. Several TPR peaks below 500 °C imply that various Ni oxide species with different sizes interact with the support. Generally, the low-temperature TPR peak in the TPR pattern for the supported Ni oxide sample can be ascribed to the reduction of bulk NiO interacting weakly with the support and the high-temperature TPR peak is due to the reduction of the well-dispersed NiO which is binding strongly onto the support. The intensities of these peaks increase with increasing Ni content from 10 to 20 wt% without the formation of new TPR peaks. The weak TPR peak at 665 °C observed for Ni/SiC-WI is attributed to the reduction of surface nickel silicate strongly interacting with SiC [31]. It is worth noting that most Ni oxides in the supported Ni catalysts prepared by WI can be reduced at 500 °C. Conversely, in the case of the catalysts prepared by DP, a single TPR pattern is obtained at a temperature higher than those of the catalysts prepared by the WI method. This indicates that the interactions between the Ni oxides and the support are stronger in the Ni catalysts prepared by DP than in those prepared by WI. It is worth mentioning that the presence of nickel antigorite ($Ni_3Si_2O_5(OH)_4$) was confirmed by XRD for the calcined Ni/SiO_2-DP sample. Ni/SiC-DP presents a TPR peak at a lower temperature than that for Ni/SiO_2-DP. Unlike the Ni catalysts prepared by WI, which can be fully reduced at 500 °C, the Ni catalysts prepared by DP are only partially reduced at the same temperature and need to be reduced at a higher temperature to increase the degree of reduction for the Ni oxide species. Nevertheless, the Ni dispersions of the catalysts prepared by DP are higher than those of the catalysts prepared by WI (Table 1). This is closely related to the difference in the dispersion of nickel oxide in the calcined catalysts (Fig. S3). The Ni dispersions of Ni/SiC-DP and Ni/

SiO_2-DP catalysts reduced at 600 °C were determined to be 11 and 8.3%. This implies that Ni dispersion increases with increasing reduction temperature from 500 to 600 °C, which is closely related to the increased degree of reduction for the Ni oxide species based on the H_2-TPR pattern (Fig. 2). Since the crystallite size of Ni in the Ni/SiO_2-DP and Ni/SiC-DP catalysts cannot be determined by XRD, TEM images were obtained to investigate the particle size of the Ni metal particles for each catalyst. As shown in Fig. 3, well-dispersed Ni particles are observed for all the supported Ni catalysts prepared by DP. The average particle sizes for Ni/SiO_2-DP, Ni/SiO_2-DP (600), Ni/SiC-DP, and Ni/SiC-DP (600) are 4.5, 4.9, 5.6, and 5.2 nm, respectively (Fig. S4).

3.2 Catalytic Performance in CO and CO_2 Methanation

The performances of the catalysts for CO and CO_2 methanation were evaluated over supported Ni catalysts prepared by WI. Figure 4a shows that the low-temperature catalytic activity for CO methanation decreases in the order 20Ni/SiO_2-WI > 20Ni/SiC-WI > 10Ni/SiO_2-WI > 10Ni/SiC-WI. This order is closely related to that of the catalytically active surface areas (CASAs) given in Table 1. Thus, a higher CASA guarantees a higher catalytic activity for CO methanation. Methane is the major product of CO methanation at all reaction temperatures (Fig. S5). The yield of ethane increases with increasing CO conversion and reaches a maximum value, after which it decreases with further increase in reaction temperature (Fig. S5). The maximum ethane yield is observed at intermediate CO conversion. Note that the yield of ethane is much lower for Ni/SiC-WI than that for Ni/SiO_2-WI (Fig. S5). The formation of propane is observed only for the most active 20Ni/SiO_2-WI catalyst (Fig. S5). In the case of CO_2 methanation (Fig. 4b), the low-temperature catalytic activity decreases in the order 20Ni/SiO_2-WI ~ 10Ni/SiO_2-WI > 20Ni/SiC-WI > 10Ni/SiC-WI. Unlike CO methanation, no close correlation between catalytic activity for CO_2 methanation and CASA is observed. This implies that there is another factor that is more important than Ni dispersion for catalytic activity in CO_2 methanation. Methane is observed as the only product during CO_2 methanation over all these catalysts except for 10Ni/SiO_2-WI, over which the formation of small amounts of CO is observed (Fig. S6). This might

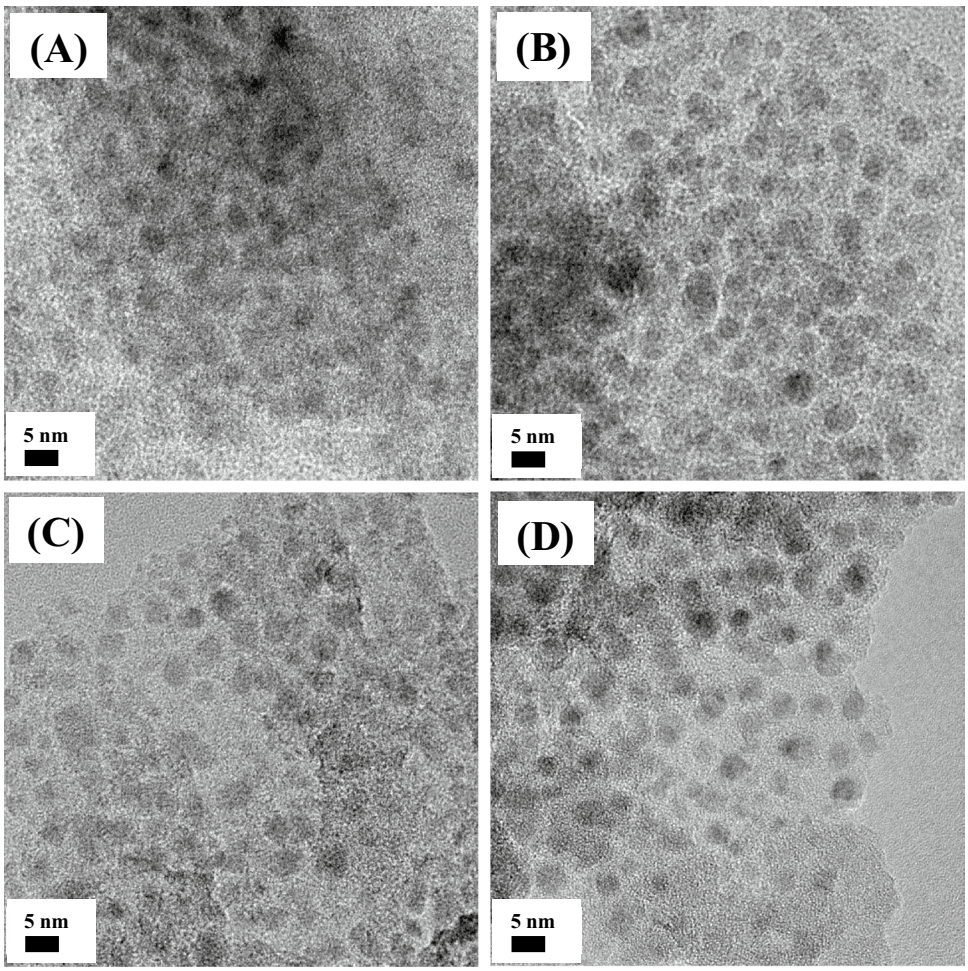

Fig. 3 TEM images of 20Ni/SiO_2-DP (**a**), 20Ni/SiO_2-DP (600) (**b**), 20Ni/SiC-DP (**c**), and 20Ni/SiC-DP (600) (**d**)

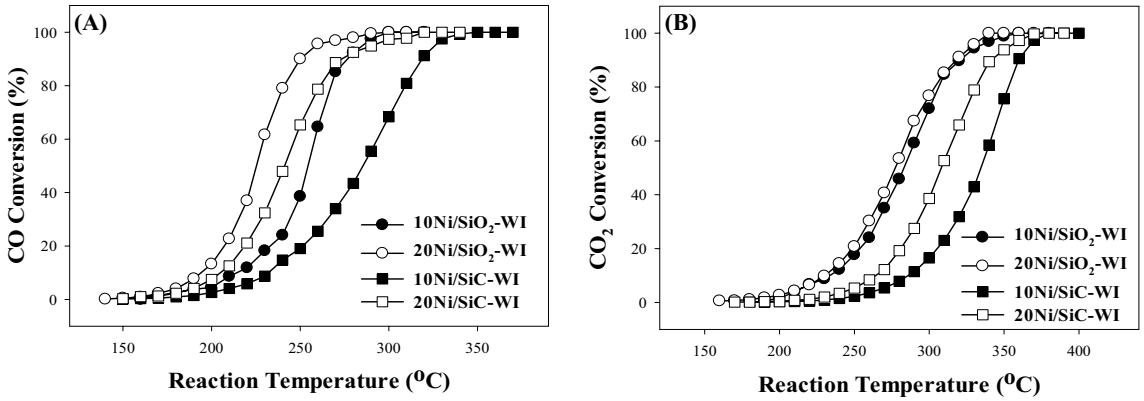

Fig. 4 Catalytic performances of supported Ni catalysts prepared by WI for CO methanation (**a**) and CO_2 methanation (**b**). All the catalysts were calcined in air at 500 °C and reduced at 500 °C. Reaction conditions: 1 mol% CO_z, 50 mol% H_2, 49 mol% He, F/W = 1000 mL/min/g_{cat}

be related to the fact that, unlike the other catalysts, which have higher catalytic activities for CO methanation than for CO_2 methanation, the 10Ni/SiO_2-WI catalyst has comparable activities in both CO methanation and CO_2 methanation.

The catalytic performances for CO and CO_2 methanation of the supported Ni catalysts prepared by DP were also evaluated. Figure 5a shows that the Ni/SiC-DP catalyst is superior to the Ni/SiO_2-DP catalyst when both catalysts are reduced at the same temperature. The 20Ni/SiC-DP catalyst exhibits better catalytic performance for CO methanation than that of the 20Ni/SiO_2-WI catalyst, which is the most active of the Ni catalysts prepared by WI. A higher catalytic activity for CO methanation with increasing reduction temperature is observed for the Ni/SiC-DP and Ni/SiO_2-DP catalysts. These results are closely related to the increase in Ni dispersion with reduction temperature. Methane is the major product of CO methanation at all reaction temperatures (Fig. S7). The formation of ethane is also observed over all the catalysts prepared by DP. However, the Ni/SiO_2-DP catalysts produce much smaller amounts of ethane than the Ni/SiO_2-WI catalysts. In the case of CO_2 methanation, the Ni/SiC-DP and Ni/SiO_2-DP catalysts exhibit similar catalytic activities, except for Ni/SiC-DP reduced at 500 °C (Fig. 5b). This clearly demonstrates that Ni dispersion and catalytically active surface area do not fully explain catalytic activity for CO_2 methanation. To resolve this issue, CO_2 uptake at room temperature and its adsorption strength on the catalyst were investigated using pulsed CO_2 chemisorption and TPD, respectively. The CO_2 uptakes for 20Ni/SiO_2-WI, 20Ni/SiC-WI, 20Ni/SiO_2-DP (600), and 20Ni/SiC-DP (600) are 3.0, 0.6, 1.4, and 1.3 μmol/g, respectively. These are lower than those of Ni catalysts supported on different aluminum oxides (except for those on α-Al_2O_3) [24]. Note that the 20Ni/SiC-WI catalyst, which showed the lowest CO_2 methanation activity, has the smallest CO_2 uptake among the catalysts compared. The CO_2-TPD data reveal that the adsorption of

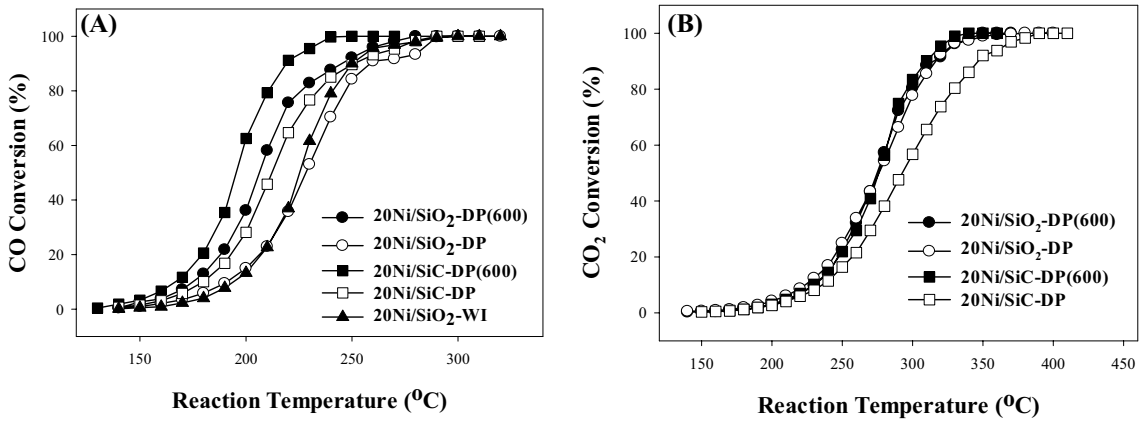

Fig. 5 Catalytic performances of supported Ni catalysts prepared by DP for CO methanation (**a**) and CO_2 methanation (**b**). For comparison, CO methanation activity data of 20Ni/SiO_2-WI are included. All the catalysts were calcined in air at 500 °C and reduced at 500 or 600 °C. Reaction conditions: 1 mol% CO_z, 50 mol% H_2, 49 mol% He, F/W = 1000 mL/min/g_{cat}

CO_2 on the SiO_2-supported Ni catalysts is stronger than that on the SiC-supported catalysts (Fig. 6). Therefore, it can be concluded that Ni dispersion as well as CO_2 adsorption capacity is essential for CO_2 methanation activity. Methane is the main product of CO_2 methanation, but the formation of CO is observed only over Ni/SiO_2-DP catalysts (Fig. S8). The longevity tests for CO and CO_2 methanation were also carried out over 20Ni/SiC-DP catalysts. The reaction temperature for each reaction was chosen not to achieve a complete conversion of CO or CO_2 in order to monitor any change in the catalytic activity. As shown in Fig. S9, there was no noticeable change in the catalytic activity for 24 h. These results reveal that the Ni/SiC catalyst prepared by DP method is stable for CO and CO_2 methanation.

3.3 Effect of Mn Promoter

Since the CO_2 uptakes for all catalysts are relatively small, the effect of support material on CO_2 methanation is limited. Therefore, Mn-promoted catalysts were prepared by DP to enhance CO_2 uptake and were applied to CO and CO_2 methanation. These catalysts have similar textural properties to those of the un-promoted Ni catalysts prepared by DP (Table 2). However, the Ni dispersions and CASAs increase upon addition of Mn (Tables 1, 2). The H_2-TPR data indicate that the presence of Mn promotes the reduction of the Ni oxide species (Fig. S10). Although the formation of metallic Ni for Mn-promoted catalysts reduced at 600 °C was confirmed based on the XRD data (Fig. S11), the crystallite size for the Ni particles cannot be determined owing to the weak peak intensity. The CO_2 uptakes at room temperature for Mn-20Ni/SiC-DP (600) and Mn-20Ni/SiO_2-DP (600) are 11 and 13 μmol/g, respectively. These are much larger than those of the un-promoted Ni catalysts. The CO_2-TPD data for the Mn-promoted Ni catalysts also confirm that the addition of Mn enhances the adsorption strength of CO_2 on the catalyst surface (Fig. S12). Consequently, Mn-promoted Ni catalysts show superior catalytic activities for CO and CO_2 methanation than those of un-promoted Ni catalysts (Fig. S13). Among the tested catalysts, Mn-promoted Ni/SiC-DP (600) exhibits the highest CO methanation activity. This catalyst also exhibits a similar CO_2 methanation activity to those of Mn-promoted Ni/SiO_2-DP (600) catalysts. The catalytic activities for CO and CO_2 methanation of all the catalysts presented in this work are compared with those of other supported Ni catalysts reported previously in Table S1. For comparison, some important physicochemical properties of each catalyst are also included. The temperature achieving 50% conversion of CO, T_{50} for CO methanation, appears to be closely related to the CASA irrespective of support. The T_{50} for CO methanation decreases with increasing CASA for all catalysts. This implies that the higher catalytic activity for CO methanation can be achieved by increasing CASA of the supported Ni catalysts. In this work, the DP method and the Mn promoter are confirmed to be effective to increase the CASA for the SiO_2- and SiC-supported Ni catalysts. On the other hand, the temperature achieving 50% conversion of CO_2, T_{50} for CO_2 methanation, is mainly dependent on CASA as well as CO_2 uptake. Additionally, the moderate adsorption strength of CO_2 was also claimed to be essential for high catalytic activity for CO_2 methanation [24].

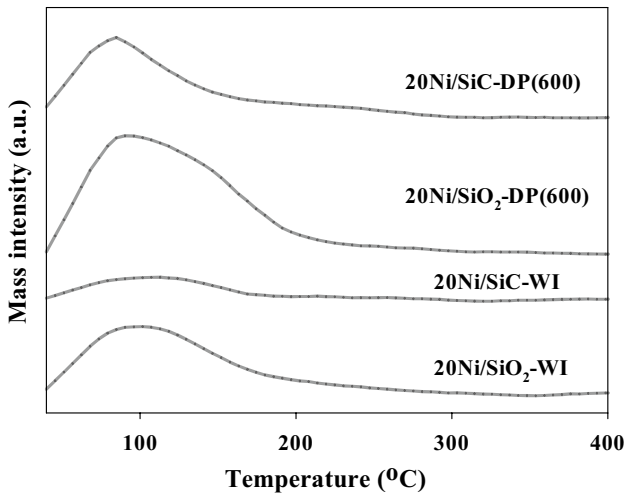

Fig. 6 CO_2-TPD patterns of the supported Ni catalysts such as 20Ni/SiO_2-WI, 20Ni/SiC-WI, 20Ni/SiO_2-DP (600), and 20Ni/SiC-DP (600)

Table 2 Physicochemical properties of Mn-promoted supported Ni catalysts

Catalyst	Specific surface area (m^2/g)[a]	Pore volume (cm^3/g)[a]	Average pore diameter (nm)[a]	Ni dispersion (%)[b]	CASA ($m^2/g_{cat.}$)[b]	CO_2 uptake (μmol/g)[c]
Mn-20Ni/SiO_2-DP	389	0.52	5	9.0	12.0	13.0
Mn-20Ni/SiC-DP	132	0.46	14	11.2	15.0	11.0

All the catalysts were calcined in air at 500 °C and reduced in hydrogen at 600 °C

[a]The specific surface area, pore volume, and average pore diameter were determined by N_2 physisorption

[b]The Ni dispersion and catalytically active surface area (CASA) were determined based on the H_2 chemisorption data

[c]The CO_2 uptake was determined based on the CO_2 chemisorption data at RT

4 Conclusion

H_2-TPR confirmed that the Ni catalyst prepared by DP exhibits stronger interaction between the nickel oxides and the support material than those prepared by WI. The former catalyst has a higher Ni dispersion than that of the latter. The catalytic activities for CO and CO_2 methanation increase with Ni content from 10 to 20 wt% over Ni/SiC and Ni/SiO_2 catalysts prepared by WI. The Ni/SiC catalyst prepared by DP shows superior catalytic activities for CO and CO_2 methanation than those of the Ni/SiC catalyst prepared by WI. Furthermore, it exhibited the highest catalytic activity for CO methanation among the tested catalysts. The high Ni dispersion achieved by the DP method coupled with the high thermal conductivity enabled by SiC are beneficial both for CO and CO_2 methanation. Further enhancements in the catalytic activities for CO and CO_2 methanation were achieved by the addition of Mn to the supported Ni catalysts owing to the increased Ni dispersion, CO_2 uptake, and adsorption strength of CO_2 on the catalyst surface.

Acknowledgements This work was supported by the Human Resources Program in Energy Technology (No. 20154010200820) of the Korea Institute of Energy Technology Evaluation and Planning (KETEP), which is granted financial resources from the Ministry of Trade, Industry and Energy of the Republic of Korea. This work was also supported by Basic Science Research Program through the National Research Foundation of Korea (NRF) funded by the Ministry of Science and ICT (2017R1A2B3011316).

References

1. Kopyscinski J, Schildhauer TJ, Biollaz SMA (2010) Fuel 89:1763–1783
2. Ahrenfeldt J, Thomsen TP, Henriksen U, Clausen LR (2013) Appl Thermal Eng 50(2):1407–1417
3. Götz M, Lefebvre J, Mörs F, Koch AM, Graf F, Bajohr S, Reimert R, Kolb T (2016) Renew Energy 85:1371–1390
4. Rönsch S, Schneider J, Mathischke S, Schluter M, Gotz M, Lefebvre J, Prabhakaran P, Bajohr S (2016) Fuel 166:276–296
5. Miao B, Ma SSK, Wang X, Su H, Chan SH (2016) Catal Sci Technol 6:4048–4058
6. Gao J, Liu Q, Gu F, Liu B, Zhong Z, Su F (2015) RSC Adv 5:22759–22776
7. Su X, Xu J, Liang B, Duan H, Hou B, Huang Y (2016) J Ener Chem 25(4):553–565
8. Aziz MAA, Jalil AA, Triwahyono S, Ahmad A (2015) Green Chem 17:2647–2663
9. Wang W, Wang S, Ma X, Gong J (2011) Chem Soc Rev 40:3703–3727
10. Ban H, Li C, Zhang Y, Meng F, Zheng H, Li Z (2015) Rev Adv Sci Eng 4:126–135
11. Shcherban ND (2017) J Ind Eng Chem 50:15–28
12. Duong-Viet C, Ba H, El-Berrichi Z, Nhut JM, Ledoux MJ, Liu Y, Pham-Huu C (2016) New J Chem 40:4285–4299
13. Ledoux MJ, Pham-Huu C (2001) CATTECH 5:226–246
14. Nguyen P, Pham C (2011) Appl Catal A 391:443–454
15. Liu Y, Ersen O, Meny C, Luck F, Pham-Huu C (2014) ChemSusChem 7(5):1218–1239
16. Wang H, Schmack R, Paul B, Albrecht M, Sokolov S, Rummler S, Kondratenko EV, Kraehnert R (2017) Appl Catal A 537:33–39
17. Hoffmann C, Plate P, Steinbrück A, Kaskel S (2015) Catal Sci Technol 5:4174–4183
18. Kim AR, Lee HY, Lee DH, Kim BW, Chung CH, Moon DJ, Jang EJ, Pang C, Bae JW (2015) Energy Fuels 29:1055–1065
19. Lakshmanan P, Kim MS, Park ED (2016) Appl Catal A 513:98–105
20. Le TA, Kim TW, Lee SH, Park ED (2018) Catal Today 303:159–167
21. Wu HC, Chang YC, Wu JH, Lin JH, Lin IK, Chen CS (2015) Catal Sci Technol 5:4154–4163
22. Xu L, Wang F, Chen M, Zhang J, Yuan K, Wang L, Wu K, Xu G, Chen W (2016) RSC Adv 6:28489–28499
23. Le TA, Kim MS, Lee SH, Kim TW, Park ED (2017) Catal Today 293:89–96
24. Le TA, Kim TW, Lee SH, Park ED (2017) Korean J Chem Eng 34(12):3085–3091
25. Zhang G, Sun T, Peng J, Wang S, Wang S (2013) Appl Catal A 462–463:75–81
26. Jin G, Gu F, Liu Q, Wang X, Jia L, Xu G, Zhong Z, Su F (2016) RSC Adv 6:9631–9639
27. Anmin Z, Weiyong Y, Haitao Z, Hongfang M, Dingye F (2012) J Nat Gas Chem 21:170–177
28. Xiaopeng L, Fangna G, Qing L, Jiajian G, Lihua J, Guangwen X, Ziyi Z, Fabing S (2015) Ind Eng Chem Res 54:12516–12524
29. Patterson A (1939) Phys Rev 56(10):978–982
30. Thommes M, Kaneko K, Neimark AV, Olivier JP, Reinoso FR, Rouquerol J, Sing KSW (2015) Pure Appl Chem 87(9–10):1051–1069
31. Jesús MGV, José LV, Antonio de LC, Beatriz GM, Paula S, Fernando D (2012) Appl Catal A 431–432:49–56